processes

MDPI

Article

Experimental Investigation of Very High Cycle Fatigue and Fatigue Crack Growth Behaviors of X17CrNi15-2 Stainless Steel

Ran Li [1,2,3,4,*], Fengcai Liu [1], Mengyu Wu [2,3], Wenshu Wei [2,3], Yuehua Lai [1,2,3], Hao Liu [2,3], Jian Ye [2,3], Tianze Cao [1], Jianfeng Li [2,3] and Wenbo Li [1]

[1] China Coal Research Institute, Beijing 100013, China
[2] State Key Laboratory of Intelligent Coal Mining and Strata Control, Beijing 100013, China
[3] Beijing Tianma Intelligent Control Technology Co., Ltd., Beijing 101399, China
[4] College of Mechanical and Electronic Engineering, Shandong University of Science and Technology, Qingdao 266590, China
* Correspondence: ranli03@163.com

Abstract

Understanding the fatigue behavior of materials is essential for designing components capable of enduring prolonged use under varying stress conditions. This study investigates the high-cycle fatigue and fatigue crack growth characteristics of X17CrNi15-2 stainless steel. Very high-cycle fatigue (VHCF) and fatigue crack growth tests were conducted on conventional fatigue and compact tension (CT) specimens fabricated from X17CrNi15-2 stainless steel. The fatigue crack growth behavior of the CT specimens was analyzed using Paris' law. A revised version of Paris' law was suggested based on the fatigue crack growth rate plotted against the stress intensity factor range, expanding on prior research utilizing three-point single-edge notch bend specimens. Scanning electron microscopy (SEM) was employed to examine the fracture mechanisms of both fatigue specimen types. The results indicated that the fatigue specimens failed in the VHCF regime under stress amplitudes ranging from 100 to 450 MPa. A power law correlation between stress amplitude and fatigue life was established, with material constants of 7670.3954 and −0.1663. These findings offer valuable insights into the material's performance and are crucial for enhancing its suitability in engineering applications where high-cycle fatigue is a critical factor.

Keywords: very-high-cycle fatigue; fatigue crack growth; Pairs' law; scanning electron microscopy; X17CrNi15-2

check for updates

Academic Editor: Chin-Hyung Lee

Received: 20 August 2025
Revised: 12 September 2025
Accepted: 19 September 2025
Published: 20 September 2025

Citation: Li, R.; Liu, F.; Wu, M.; Wei, W.; Lai, Y.; Liu, H.; Ye, J.; Cao, T.; Li, J.; Li, W. Experimental Investigation of Very High Cycle Fatigue and Fatigue Crack Growth Behaviors of X17CrNi15-2 Stainless Steel. *Processes* **2025**, *13*, 3004. https://doi.org/10.3390/pr13093004

Copyright: © 2025 by the authors. Licensee MDPI, Basel, Switzerland. This article is an open access article distributed under the terms and conditions of the Creative Commons Attribution (CC BY) license (https://creativecommons.org/licenses/by/4.0/).

1. Introduction

High-pressure reciprocating pumps commonly utilize high-strength martensitic stainless steels for components like liquid ends [1]. These stainless steel parts undergo high-frequency, low-stress amplitude cyclic loading, exceeding 10^7 cycles in service life, demonstrating very high cycle fatigue (VHCF) behavior. Failures of these components are typically linked to the propagation of inclusions or initial crack-like flaws. Reciprocating pumps commonly employ emulsion as their primary hydraulic fluid, which is predominantly water-based. The challenging conditions of high temperatures and humidity in underground mining settings are recognized to influence the fatigue and crack propagation of stainless steel, consequently leading to pump component failure and damage. Research shows that at 85% relative humidity (RH), the fatigue strength of martensitic steel decreases to less than 50% of its value at 25% RH, accompanied by a notable rise in crack propagation rate. Moreover, the crack surface transitions to a smoother texture under elevated humidity

levels, manifesting concave regions in martensitic steel at 85% RH, while displaying a rougher appearance at lower humidity levels [2]. In high-temperature aqueous settings, the combined influence of humidity and temperature accelerates crack propagation in 316LN stainless steel, with heightened oxidation contributing to an increased acceleration factor [3]. Therefore, studying VHCF and fatigue crack growth behavior is crucial for assessing the remaining service life of such components. Defect tolerance design methods are frequently applied in this context.

X17CrNi15-2 stainless steel is a suitable material for reciprocating pumps due to its superior hardness, tensile strength, corrosion resistance, and weldability [4]. In the VHCF regime, fatigue cracks typically originate from internal inclusions before extending, creating a distinct fish-eye pattern with a "fine granular area" (FGA) adjacent to the inclusion [5]. This FGA is also known as the "optically dark area" (ODA) [6] or "granular bright facet" (GBF) [6]. Krupp et al. [7] conducted ultrasonic VHCF tests on a duplex stainless steel (DSS) 1.4462 and demonstrated that the spinodal decomposition of ferrite improves VHCF strength. Sun et al. [8] studied the FGA size and assessed the equivalent crack growth rate in the FGA during VHCF of martensitic stainless steel AISI630. Li et al. [9] observed that fatigue cracks initiate at the martensite lath boundaries, resulting in a slip area at the center of the FGA in super martensitic stainless steel 0Cr13Ni5Mo under VHCF conditions. Furthermore, Zheng et al. [10] discovered that varying aging times in a precipitation hardening martensitic stainless steel in the VHCF regime can lead to two fatigue crack initiation mechanisms—inclusion-induced and non-inclusion-induced crack initiation. Karr et al. [11] found that VHCF cracks in martensitic steels often originate from nonmetallic inclusions (such as Al_2O_3, TiN, and Zr(N,C)). Among these, TiN inclusions exhibit the strongest stress concentration effect, significantly reducing fatigue strength. By optimizing composition—such as reducing Ti content and increasing Al—crack initiation can be promoted at less destructive Al_2O_3 inclusions, thereby enhancing VHCF performance. Wang et al. [12] concluded through research that fatigue failure in high-strength martensitic stainless steels (such as FV520B-I) is predominantly triggered by internal inclusions, with crack initiation locations directly correlated to inclusion size and stress concentration levels. Song et al. [13] found that early crack propagation under VHCF is associated with grain refinement caused by interaction with dislocations. TEM observations revealed discontinuous fine-grain zones near cracks, whereas no grain refinement was observed in compression fatigue tests, indicating that this mechanism is related to tensile loading.

Fan et al. [14] conducted fatigue crack growth tests on round compact specimens made of stainless steel 304, introducing a new finite element approach based on damage mechanics. Nie and Mutoh [15] adapted the Basquin equation to describe the S-N curve in the VHCF regime and studied fatigue crack growth in precipitation-hardening martensitic stainless steel 17-4PH. Chai et al. [16] utilized acoustic emission entropy for precise fatigue damage assessment and fatigue crack length prediction. Kamaya [17] analyzed the fitness-for-service (FFS) fatigue growth rates of solution-heat-treated type 316 austenitic stainless steel in accordance with the Japanese Society of Mechanical Engineers FFS (JSME FFS) code, incorporating temperature effects. Sajith et al. [18] performed mixed-mode (I/II) fatigue crack growth tests on compact tension shear specimens consisting of AISI 316 austenitic stainless steel at varying loading angles.

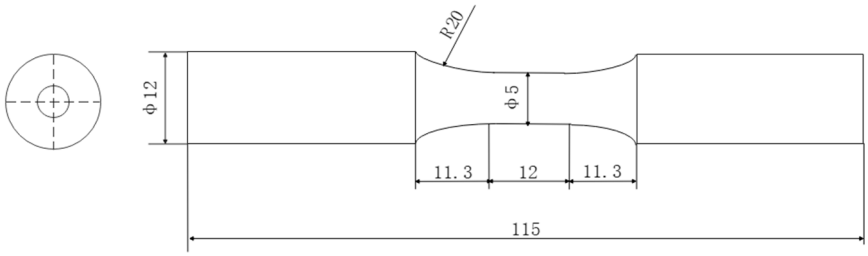
In this study, VHCF and fatigue crack growth tests were performed on two types of stainless steel fatigue specimens (X17CrNi15-2)—conventional fatigue specimens and compact tension (CT) specimens. The stress–fatigue life relationship was determined by fitting the VHCF S-N data. Fatigue crack growth behavior was analyzed using Paris' law, derived from curve fitting fatigue crack growth rate against stress intensity factor data. A revised Paris' law was developed using test data from CT specimens in this study and SEN

B3 specimens from prior research. Fracture mechanisms of VHCF and CT specimens were investigated through scanning electron microscopy (SEM).

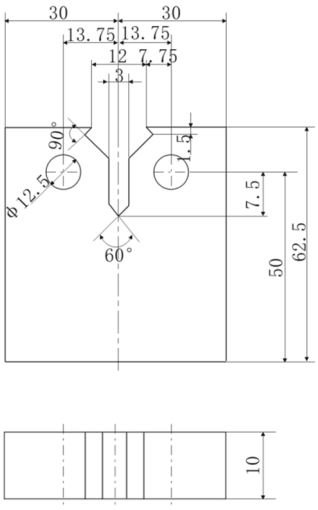
2. Experimental

2.1. Test Material and Specimens

The chemical composition of X17CrNi15-2 martensitic stainless steel was analyzed, revealing the following composition (wt. %): 0.769 Si, 0.106 V, 16.290 Cr, 0.409 Mn, 0.215 Co, 1.970 Ni, 0.259 Cu, 0.017 Zn, 0.181 Mo, 0.015 Sn, 0.099 S, and Fe balance. Two types of fatigue test specimens, namely conventional fatigue specimens and standard CT specimens, were employed to study the short-crack growth behavior of the X17CrNi15-2 stainless steel. The specimens' dimensions adhered to the requirements outlined in GB/T 43896-2024 [19] and ISO 12108-2018 [20] standards (Figure 1). The conventional fatigue specimens featured a 12 mm diameter necking down to 5 mm (Figure 1a). CT specimens were pre-cracked using the cycle-loading method, with all specimens having a notch length (a_n) of 7.5 mm, thickness (B) of 10 mm, and width (W) of 50 mm (Figure 1b). The fatigue crack length (a_o) was measured from the notch root, a_n, spanning up to 3 mm. The roughness of the six external surfaces (front, back, left, right, top, bottom) of the CT test specimen is specified as Ra 0.8, while the inner wall surfaces of the two 12.5 mm diameter holes on the left and right sides are also specified as Ra 0.8. All other surfaces are specified to have a roughness of Ra 1.6. Limiting the fatigue pre-crack length during pre-cracking ensures consistent crack tip geometry. SEM images confirm the repeatability of crack dimensions and locations [21,22].



(**a**) The tension–compression fatigue specimens



(**b**) The standard CT specimens.

Figure 1. The dimensions of specimens: (**a**) The dimensions of the tension-compression fatigue specimens; (**b**) The dimensions of the standard CT specimens.

2.2. Test Apparatus and Procedure

VHCF tests were conducted on conventional fatigue specimens using the ZwickRoell Vibrophore 100 (ZwickRoell, Ulm, Germany) high-frequency fatigue testing machine, with

a stress ratio of -1 (Figure 2a). The high-pressure plunger pumps can operate at pressures of 80–100 MPa, potentially leading to local stresses surpassing 100 MPa due to factors like stress concentration and surface quality. Hence, a fatigue test was designed with nine stress amplitude levels from 100 MPa to 500 MPa to account for these variations. Each stress level underwent three independent fatigue tests to minimize scatter effects.



(**a**) ZwickRoell Vibrophore 100 high-frequency fatigue testing machine



(**b**) MT810 material testing system

Figure 2. Test apparatus: (**a**) ZwickRoell Vibrophore 100 high-frequency fatigue testing machine; (**b**) MT810 material testing system.

The CT specimens (Figure 2b) were tested using the MT810 (MTS, Eden Prairie, MN, USA) material testing system. Fatigue crack growth tests were conducted with a stress ratio of 0.5 and a frequency of 50 Hz, applying sine-wave load profiles. The maximum load values (P_{max}) ranged from 3.5 to 5.5 kN. Crack length measurements were performed with a crack-opening displacement gauge, offering an accuracy of 0.001 mm.

3. Results and Analyses

3.1. S-N Data for VHCF

Figure 3 illustrates the S-N data for conventional fatigue specimens subjected to varying stress amplitude levels. The test conditions and results of the VHCF tests are detailed in Table 1. Fatigue lives exceeding 10^7 cycles were observed for stress amplitudes ranging from 100 MPa to 450 MPa. The transition from VHCF to HCF regime occurs as the stress amplitude level reaches 500 MPa. Curve fitting of the VHCF S-N data was performed using a power-law relationship akin to the Basquin equation [23] presented in Equation (1):

$$\sigma_a = 7670.3954\left(N_f\right)^{-0.16633} \quad (1)$$

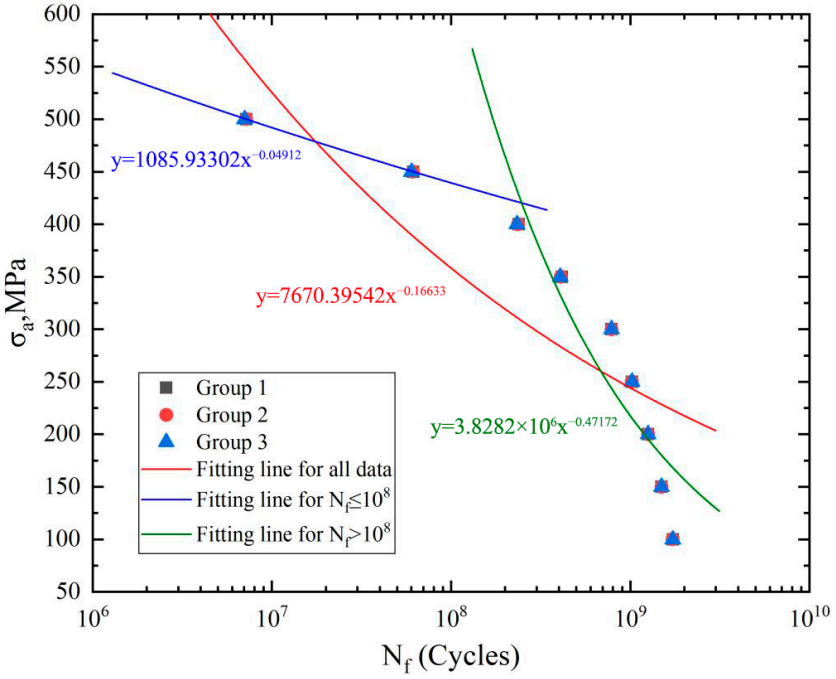


Figure 3. S-N data for the conventional fatigue specimens under different levels of stress amplitude.

Table 1. Test conditions and results of the VHCF tests.

Mean Stress (MPa)	Fatigue Lives N (Cycles)		
	Group 1	Group 2	Group 3
100	1,728,092,773	1,728,067,856	1,728,070,000
150	1,492,734,787	1,492,728,658	1,492,730,000
200	1,257,419,343	1,257,397,177	1,257,400,000
250	1,022,075,054	1,022,058,218	1,022,060,000
300	786,748,915	786,719,456	786,722,000
350	415,000,000	411,000,000	407,000,000
400	238,000,000	237,000,000	233,000,000
450	61,500,000	61,300,000	60,100,000
500	7,200,000	7,170,000	7,040,000

A significant scatter was noted in the curve fitting of the complete VHCF S-N data to establish the power law relationship (Figure 3). Utilizing a piecewise function may offer a more precise depiction of the VHCF life behavior, as illustrated in Equation (2).

$$\sigma_a = \begin{cases} 1085.933\left(N_f\right)^{-0.04912} & for\ N_f \le 10^8 \\ 3.8282 \times 10^6\left(N_f\right)^{-0.47172} & for\ N_f > 10^8 \end{cases} \quad (2)$$

3.2. Fatigue Crack Growth

Figure 4 illustrates the relationship between fatigue crack lengths and the number of cycles for applied forces of 3.5 kN, 4.5 kN, and 5.5 kN (All data in the figure were obtained directly from the testing machine's measurement system). In accordance with ISO 12108-2018 guidelines, the stress-intensity factor K can be determined by utilizing the applied forces and the corresponding crack lengths derived from fatigue crack growth tests using Equation (3):

$$K = \frac{F}{B\sqrt{W}} g\left(\frac{a}{W}\right) \quad (3)$$

where F represents the applied force; B denotes the specimen thickness; W signifies the specimen thickness measured from the reference plane to the specimen edge; a indicates the crack length; and $g\left(\frac{a}{w}\right)$ represents the stress-intensity factor geometry.

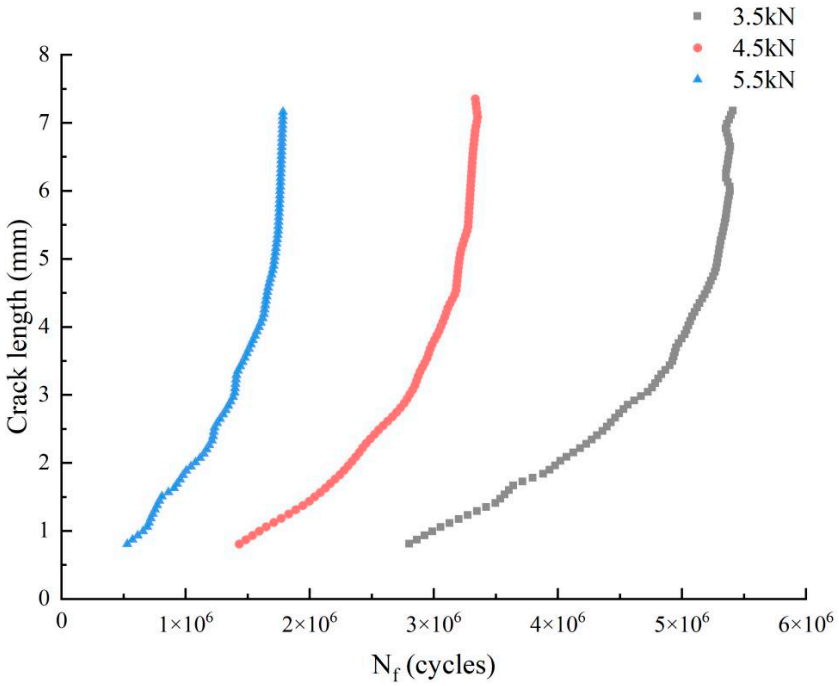


Figure 4. Fatigue crack lengths versus the number of cycles for three maximum applied forces.

For the CT specimen configuration, $g\left(\frac{a}{W}\right)$ can be obtained by Equation (4)

$$g\left(\frac{a}{W}\right) = \frac{(2+\alpha)\left(0.886 + 4.64\alpha - 13.32\alpha^2 + 14.72\alpha^3 - 5.6\alpha^4\right)}{(1-\alpha)\sqrt{1-\alpha}} \quad (4)$$

where $\alpha = \frac{a}{W}$

The fatigue crack growth behavior of the X17CrNi15-2 martensitic stainless steel can be characterized using Paris' law, a widely applied power law correlation between crack growth rates ($\frac{da}{dN}$) and stress-intensity factor ranges (ΔK), as expressed in Equation (5):

$$\frac{da}{dN} = C(\Delta K)^m \quad (5)$$

where C and m are material constants.

Figure 5 illustrates the correlation between fatigue crack growth rates ($\frac{da}{dN}$) and stress intensity factor ranges (ΔK) on a log-log scale. A linear regression was performed on the data to determine the material constants C and m in Paris' law, resulting in values of 2.071×10^{-16} and 6.007, respectively. Therefore, the Paris' law equation for X17CrNi15-2 martensitic stainless steel is expressed as

$$\frac{da}{dN} = 2.071 \times 10^{-16}(\Delta K)^{6.007} \quad (6)$$

A study previously examined the impact of ceramic coating on the fatigue crack growth behavior of X17CrNi15-2 stainless steel through three-point single-edge notch bend (SEN B3) specimens at R = 0.1 [4]. The fatigue crack growth data obtained from the CT specimens were compared with those from the SEN B3 specimens in the aforementioned study [4] (Figure 6). In Figure 6, the ΔK values for SEN B3 specimens ranged from 25 to

77 MPa·m$^{1/2}$, where as for CT specimens, they ranged from 43 to 75 MPa·m$^{1/2}$. The test data from SEN B3 specimens were situated at the lower end of the test data from the CT specimens at $\Delta K > 40$ MPa·m$^{1/2}$. A new power law relationship between crack growth rates ($\frac{da}{dN}$) and stress intensity factor ranges (ΔK) was established using data from both the CT and SEN B3 tests, as represented in Equation (7):

$$\frac{da}{dN} = 8.559 \times 10^{-16} (\Delta K)^{5.531} \quad (7)$$

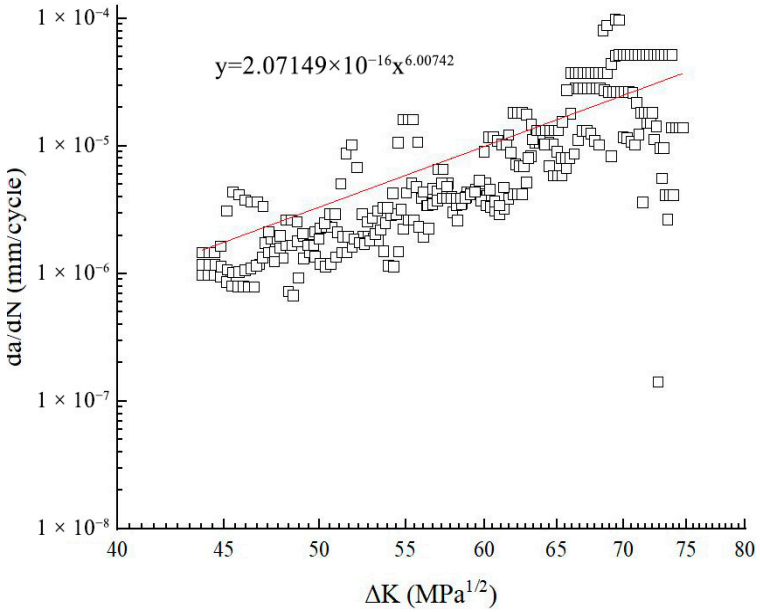


Figure 5. Fatigue crack growth rates versus stress intensity factor ranges data using CT specimens.

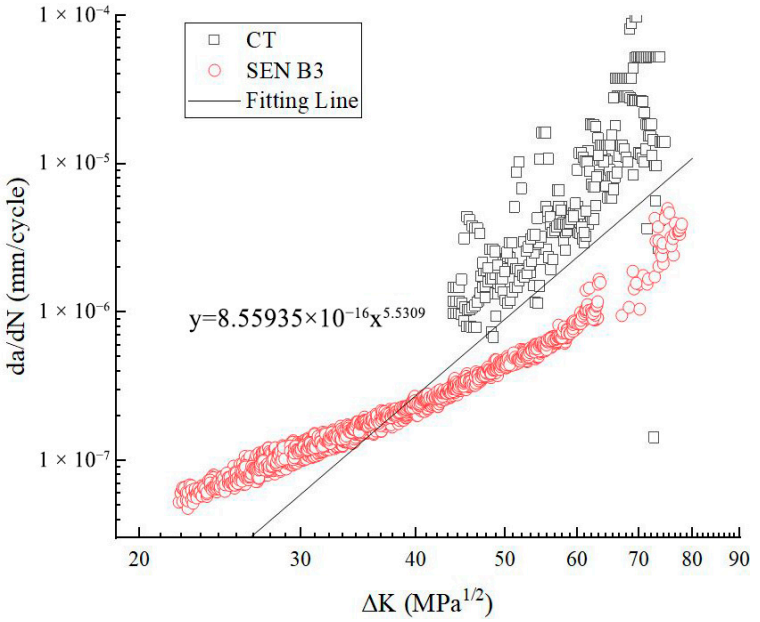


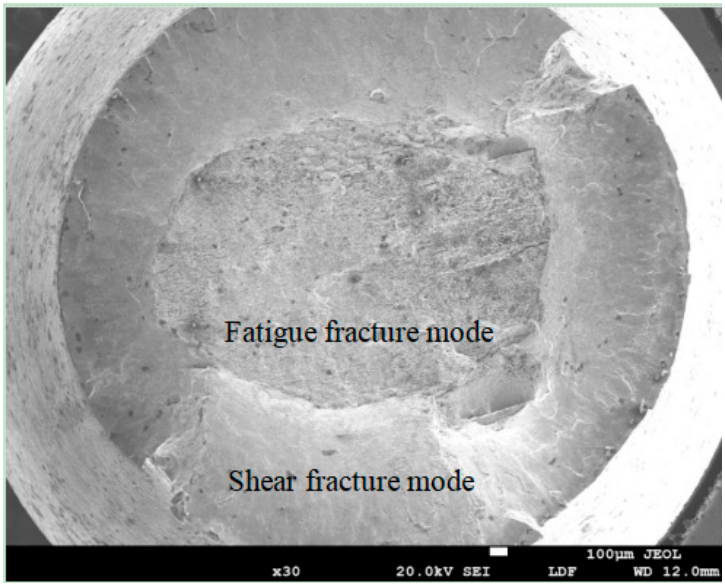
Figure 6. Fatigue crack growth rates versus stress intensity factor ranges data using CT specimens and SEN B3 specimens.

The stress amplitude range designated for VHCF testing is 100–500 MPa, considering stress concentration and related variables. Nevertheless, specimens tested at 500 MPa stress amplitude, as depicted in Figure 3, displayed cycle counts below 10^7, failing to reach the

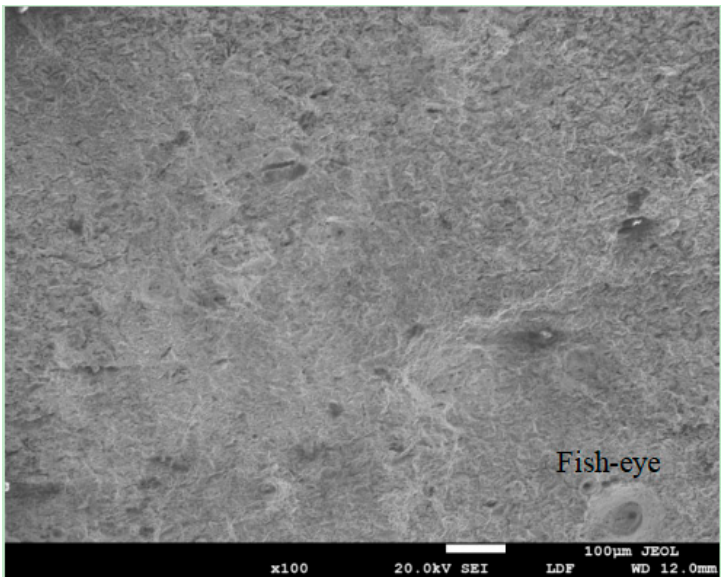
ultra-high-cycle fatigue regime. This discrepancy could introduce bias, thereby impacting the adjusted prediction outcomes based on Paris's law.

3.3. SEM Morphology Analyses

SEM analysis was conducted on the fracture zones of VHCF and CT specimens. Figure 7a illustrates the SEM fracture surface of the VHCF specimen tested, revealing two distinct fracture modes: fatigue fracture and shear fracture. Figure 7b displays identifiable fish-eye patterns that indicate multiple crack initiation locations, aligning with crack initiation behavior under smaller stress amplitudes and longer cyclic loading. Fracture stress concentration zones (FGA) are evident around the fish-eye patterns, contrasting with surface crack initiation patterns observed in low-cycle fatigue testing.



(**a**) A lower magnification

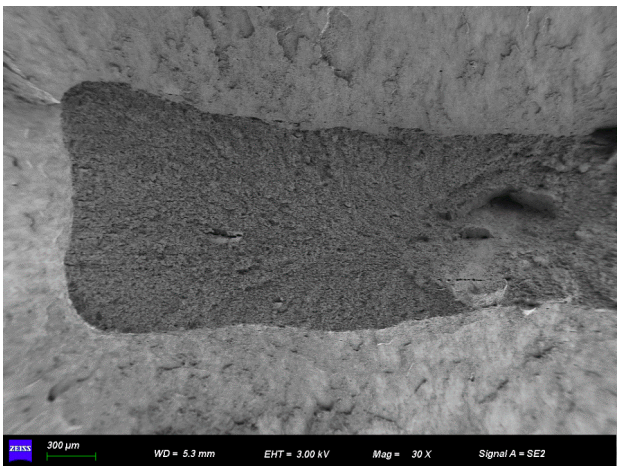


(**b**) A higher magnification

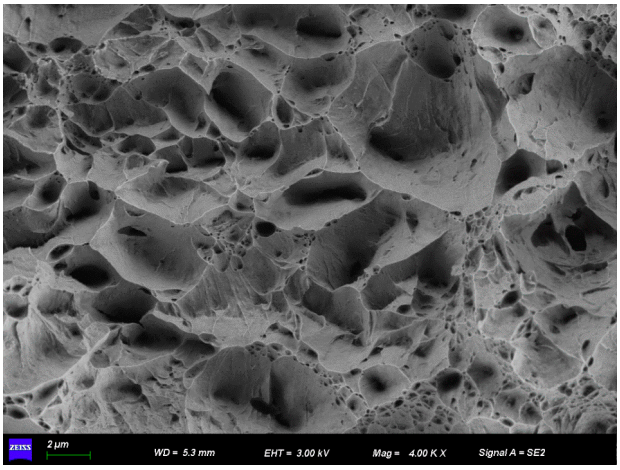
Figure 7. SEM images of the fracture surfaces of the tested VHCF specimen: (**a**) a lower magnification; (**b**) a higher magnification.

The crack initiation points in all crack propagation specimens were identified at the initial crack positions, underscoring the importance of fracture surface morphology

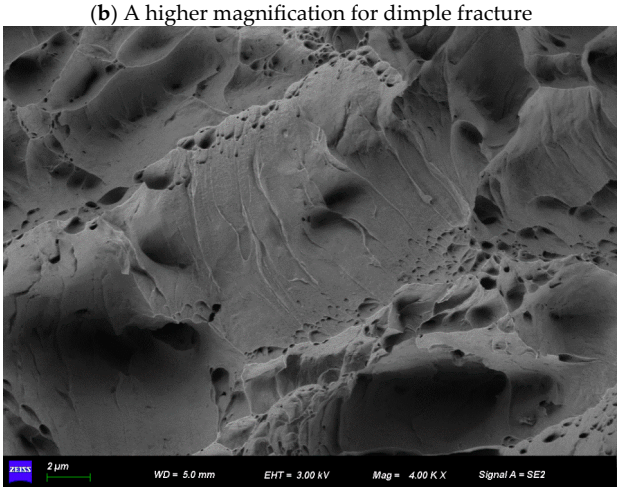
analysis in assessing fracture toughness behavior. A mixed fracture mode, characterized by a quasi-cleavage-toughening pit hybrid brittle intergranular fracture, was observed on the fracture surfaces within the crack propagation zone. This mode is defined by the combination of quasi-cleavage fracture and pit formation (refer to Figure 8). Within the crack propagation zone, quasi-cleavage fracture predominates, governing the fatigue crack propagation process. The presence of localized intergranular pitting on the fracture surface indicates the exceptional impact toughness of X17CrNi15-2 stainless steel.



(**a**) A lower magnification



(**b**) A higher magnification for dimple fracture



(**c**) A higher magnification for quasi-cleavage fracture

Figure 8. SEM images of the fracture surfaces of the tested VHCF specimen: (**a**) a lower magnification (**b**) a higher magnification for dimple fracture; (**c**) a higher magnification for quasi-cleavage fracture.

4. Conclusions

This study investigates the very-high-cycle fatigue (VHCF) and fatigue crack growth characteristics of X17CrNi15-2 stainless steel through VHCF and fatigue crack growth tests performed on conventional fatigue and standard compact tension (CT) specimens. The conclusions are as follows:

When stress amplitudes ranged from 100 to 450 MPa, fatigue specimens failed under VHCF conditions (>10^7 cycles). However, at a stress amplitude of 500 MPa, fatigue life decreased to approximately 7×10^6 cycles, indicating the transition from VHCF to HCF. A power-law model was derived to forecast stress-VHCF life, with coefficients of 7670.3954 and -0.16633. Moreover, a piecewise function was formulated to adjust VHCF behavior for cases $N_f \leq 10^8$ and $N_f > 10^8$.

The Paris law characterizes the fatigue crack propagation rate of X17CrNi15-2 CT specimens over a range of stress intensity factors, with initial parameters of C = 2.071×10^{-16} and m = 6.007. Through the integration of CT specimen data from this investigation with SEN B3 specimen data from previous studies, the law was adjusted resulting in revised values of C = 8.559×10^{-16} and m = 5.531. Nevertheless, due to the specimens not being entirely subjected to VHCF conditions within the 100–500 MPa range, the modified Paris law may demonstrate some deviation, potentially impacting prediction accuracy.

SEM analysis was conducted to characterize the fatigue fracture mechanisms of two fatigue specimens. Two distinct fracture modes were identified on the VHCF fracture surface: fatigue fracture and shear fracture. Fish-eye patterns were observed, indicating multiple crack initiation points consistent with low-amplitude, long-cycle loading characteristics. Fracture stress concentration zones were found around the fish-eye patterns, differing from the surface initiation patterns seen in low-cycle fatigue; these zones were surrounded by fine-grained regions containing inclusions or defects. The fracture surface of the CT specimen predominantly exhibited quasi-cleavage fracture during fatigue crack propagation, which governed the crack growth process. Intergranular pitting was only observed in limited areas, suggesting good impact toughness.

Due to limitations in experimental conditions, this study only performed SEM analysis and did not conduct metallographic microstructure analysis, energy dispersive spectroscopy (EDS), or image analysis. Future research will integrate additional analytical techniques to explore the material's microstructure and establish connections between fracture morphology, loading conditions, and microstructural features. Moreover, leveraging the experimental findings from this study and employing finite element simulation methods, defect-tolerant design principles will be implemented in pump components to improve the operational reliability of the plunger pump.

Author Contributions: Conceptualization, R.L. and W.W.; formal analysis, R.L.; validation, T.C., F.L. and W.L.; investigation, R.L. and M.W.; data curation, M.W., Y.L., J.Y. and J.L.; writing—original draft preparation, R.L.; writing—review and editing, H.L.; supervision, W.W.; project administration, W.W.; funding acquisition, R.L. All authors have read and agreed to the published version of the manuscript.

Funding: This research was supported by CCTEG Project (2023-TD-MS015, 2023-TD-QN004) and TMIC Project (2022TM-167M) funding, China.

Data Availability Statement: The original contributions presented in this study are included in the article. Further inquiries can be directed to the corresponding author.

Conflicts of Interest: Ran Li, Mengyu Wu, Wenshu Wei, Yuehua Lai, Hao Liu, Jian Ye and Jianfeng Li were employed by the Beijing Tianma Intelligent Control Technology Co., Ltd. The remaining authors declare that the research was conducted in the absence of any commercial or financial relationships that could be construed as a potential conflict of interest.

References

1. Miller, J.E. *The Reciprocating Pump Theory Design and Use*; Wiley: New York, NY, USA, 1987.
2. Kariya, K.; Kawagoishi, N. Effect of humidity on initiation and propagation properties of a fatigue crack of maraging steel. *Res. Rep.* **2013**, *25*, 59–67.
3. Li, C.; Li, X.; Xu, X.H.; Lv, Z.P.; Cui, T.M.; Pan, D.; Chen, J.J.; Zheng, H.; Yang, S.L.; Zhong, Z.M. Low-Frequency Corrosion Fatigue Crack Propagation Behavior of 316LN Stainless Steel at Different Temperatures. *Corros. Prot.* **2025**, *46*, 60–65. [CrossRef]
4. Li, R.; Wei, W.S.; Li, S.B.; Zhao, R.; Liu, H.; Zhang, J.K.; Ye, J.; Wu, H.G.; Xu, Y.; Xiao, F.; et al. The influence of ceramic coating on fatigue crack growth behaviour of X17CrNi15-2 stainless steel. *Engineering* **2020**, *12*, 140–149. [CrossRef]
5. Milella, P. *Fatigue and Corrosion in Metals*; Springer: Berlin/Heidelberg, Germany, 2012.
6. Murakami, Y. *Metal Fatigue: Effects of Small Defects and Nonmetallic Inclusions*; Academic Press: Cambridge, MA, USA, 2019.
7. Krupp, U.; Söker, M.; Giertler, A.; Dönges, B.; Christ, H.J.; Wackermann, K.; Boll, T.; Thuvander, M.; Marinelli, M.C. The potential of spinodal ferrite decomposition for increasing the very high cycle fatigue strength of duplex stainless steel. *Int. J. Fatigue* **2016**, *93*, 363–371. [CrossRef]
8. Sun, C.Q.; Song, Q.Y.; Zhou, L.L.; Pan, X.N. Characteristic of interior crack initiation and early growth for high cycle and very high cycle fatigue of a martensitic stainless steel. *Mater. Sci. Eng. A* **2019**, *758*, 112–120. [CrossRef]
9. Li, X.; Dai, Y.J.; Wang, X.Y.; Liu, Y.J.; Chen, Y.; Wang, C.; Zhang, H.; Li, L.; Liu, H.Q.; He, C.; et al. Effects of local microstructure on crack initiation in super martensitic stainless steel under very-high-cycle fatigue. *Int. J. Fatigue* **2022**, *163*, 107019. [CrossRef]
10. Zheng, Y.; Sun, H.L.; Yan, L.C.; Pang, X.L.; Gao, K.W. Effect of aging time on crack initiation mechanism of precipitation hardening stainless steel in very high cycle fatigue regime. *Int. J. Fatigue* **2023**, *170*, 107522. [CrossRef]
11. Karr, U.; Pennings, B.; Tran, D.; Myer, H. Development of nitrided 18Ni maraging steel to optimise the very high cycle fatigue properties. In Proceedings of the Seventh International Conference on Very High Cycle Fatigue, Dresden, Germany, 3–5 July 2017.
12. Wang, J.L.; Yang, Y.X.; Yu, J.; Wang, J.S.; Du, F.M.; Zhang, Y.L. Fatigue life evaluation considering fatigue reliability and fatigue crack for FV520B-I in VHCF regime based on fracture mechanics. *Metals* **2020**, *10*, 371. [CrossRef]
13. Song, Q.Y.; Sun, C.Q. Mechanism of crack initiation and early growth of high strength steels in very high cycle fatigue regime. *Mater. Sci. Eng. A* **2020**, *771*, 138648. [CrossRef]
14. Fan, F.F.; Kalnaus, S.; Jiang, Y.Y. Modeling of fatigue crack growth of stainless steel 304L. *Mech. Mater.* **2008**, *40*, 961–973. [CrossRef]
15. Nie, D.F.; Mutoh, Y. Fatigue limit prediction of the matrix of 17-4PH stainless steel based on small crack mechanics. *J. Press. Vessel Technol.* **2013**, *135*, 021407. [CrossRef]
16. Chai, M.Y.; Zhang, Z.X.; Duan, Q.; Song, Y. Assessment of fatigue crack growth in 316LN stainless steel based on acoustic emission entropy. *Int. J. Fatigue* **2018**, *109*, 145–156. [CrossRef]
17. Kamaya, M. Fatigue crack tolerance design for stainless steel by crack growth analysis. *Eng. Fract. Mech.* **2017**, *177*, 14–32. [CrossRef]
18. Sajith, S.; Shukla, S.S.; Murthy, K.S.R.K.; Robi, P.S. Mixed mode fatigue crack growth studies in AISI 316 stainless steel. *Eur. J. Mech. A Solids* **2020**, *80*, 103898. [CrossRef]
19. *GB/T 43896-2024*; Metallic Materials-Very High Cycle Fatigue-Ultrasonic Fatigue Test Method. China Standardization Administration: Beijing, China, 2012.
20. *ISO 12108-2018*; Metallic Materials-Fatigue Testing-Fatigue Crack Growth Method. International Organization for Standardization: Geneva, Swiss, 2018.
21. Zhang, X.; Zhang, Z.L.; Chen, Y.; Liu, Y.; Yang, X.; Zhou, F.; Rong, P.; Chen, H. Microstructure and mechanical properties of TC11 titanium alloy obtained by laser wire additive manufacturing. *J. Sichuan Univ. (Nat. Sci. Ed.)* **2025**, *62*, 785–792. [CrossRef]
22. Preston, D.; Sanmartin, D.R.; Watts, J.; Wright, J. Controlled seeding of contact cracks in test pieces for the evaluation and validation of non-destructive testing systems. *F1000Research* **2023**, *12*, 1103. [CrossRef]
23. Firdaus, S.M.; Arifin, A.; Abdullah, S.; Singh, S.S.K.; Nor, N.M. Fatigue life assessment of API steel Grade X65 pipeline using a modified Basquin parameter of the magnetic flux leakage signal. *Materials* **2023**, *16*, 464. [CrossRef] [PubMed]

Disclaimer/Publisher's Note: The statements, opinions and data contained in all publications are solely those of the individual author(s) and contributor(s) and not of MDPI and/or the editor(s). MDPI and/or the editor(s) disclaim responsibility for any injury to people or property resulting from any ideas, methods, instructions or products referred to in the content.